INSTITUTE OF PLASMA PHYSICS

NAGOYA UNIVERSITY

RESEARCH REPORT

NAGOYA, JAPAN

NONLINEAR SELF-MODULATION OF ION-ACOUSTIC WAVES

H. Ikezi*, K. Schwarzenegger* and A.L. Simons*

and

Y. Ohsawa and T. Kamimura

IPPJ-289 May 1977

Further communication about this report is to be sent to the Research Information Center, Institute of Plasma Physics, Nagoya University, Nagoya 464, Japan.

---

* Bell Laboratories, Murray Hill, New Jersey 07974

ABSTRACT

The nonlinear evolution of an ion-acoustic wave packet is studied. Experimentally we find that (i) nonlinear phase-modulation develops in the wave packet; (ii) the phase-modulation, together with the dispersion effect, causes expansion, and breaking of the wave packet; (iii) the ions trapped in the troughs of the wave potential introduce self-phase-modulation, and (iv) the ion-acoustic wave is stable with respect to the modulational instability. Computer simulations have reproduced the experimental findings. The physical picture and the model equation describing the wave evolution are discussed.

I. INTRODUCTION

The nonlinear behavior of wave packets in dispersive systems has received considerable theoretical attention.[1] A kinetic theory,[2] which considers the resonance at the group velocity, predicts that the ion-acoustic wave is unstable with respect to wave amplitude modulation, in contrast to the results of the fluid theory.[3,4] The studies to be presented in this paper were motivated by the contradiction between these two theories. We have found both experimentally and by computer simulations, that the ions trapped in the wave potential troughs introduce much larger effects compared to the mechanisms discussed in the theories.[2-4]

Experimentally, we investigate a plane ion-acoustic density perturbation of the form

$$\delta n = \tilde{n}(x,t)\exp(ik_0x - i\omega_0t), \qquad (1)$$

with the carrier wave frequency ω_0 and the wavenumber k_0. The envelope $\tilde{n}$ is a slowly varying function of space x and time t compared to the carrier oscillation period. Figure 1 shows the propagation of the wave packet for small perturbed amplitudes. It is excited at x = 0 by the signal shown in the top trace (only the

trace when $\omega_0/2\pi = 0.4$ MHz is shown). The signals detected at x = 8 cm (2nd through 5th trace) are delayed because of the transit time of the packet. The wave packet with larger ω_0 (labeled at each trace) undergoes a longer delay. This is expected since the group velocity is given by $v_g = \partial\omega/\partial k|_{\omega=\omega_0} = c_s[1 - (\omega_0/\omega_{pi})^2]^{3/2}$. In this linear regime, the envelope $\tilde{n}$ is slightly spread out without showing any additional modulation.

The evolution of the shape and phase of the packet when the amplitude is large is the subject of our interest. The experiment described in the next section demonstrates the nonlinear phase modulation. We will find that the phase modulation causes broadening of the frequency spectrum and wave packet breaking. The computer simulations presented in Section III reproduce the experimental results. In Section IV, we discuss the physical picture of the wave evolution and phenomenologically derive a model equation which describes the wave evolution. We will point out the importance of trapped-ion effects. The results of the present work are summarized in the last section.

II. EXPERIMENT

A. Apparatus and Conditions

The experiments were carried out in a double plasma device.[5] The details of the device, and the method

of wave excitation are described in Ref. 5. The typical density of the argon plasma $n_0 = (0.5 \sim 5) \times 10^9$ cm^{-3} is obtained at an argon pressure $p = (1 \sim 2) \times 10^{-4}$ Torr. The electron temperature T_e is controllable in a range from 0.5 eV to 3 eV. The Langmuir probe curves in Fig. 2 showing changes in T_e are obtained by regulating the discharge current ratio between the poorly conductive chamber wall and an additional metallic electrode which absorbs high energy electrons.[6] The ion temperature, $T_i = 0.1$ eV, is observed by an ion energy analyzer. It is roughly independent of the changes in T_e. We have also obtained T_i from measurements of the Landau damping of the ion-acoustic wave. We will use this T_i in analyzing experimental data when dealing with the trapped ion effects. The diameter of the wave front (30 cm) is much larger than the wavelength (a few mm). We have confirmed that the propagation and damping of the ion-acoustic wave in our device is well described by the dispersion relation[7]

$$1 + (k_D^2/k^2) \left[1 - (T_e/2T_i)\, Z'(\omega/kv_i)\right] = 0. \qquad (2)$$

when the amplitude is small.

B. Results

We first observe the behavior of the amplitude-modulated wave

$$\tilde{n}(x = 0, t) = \tilde{n}_0(1+\varepsilon \cos \omega_m t) , \qquad (3)$$

launched at x = 0 in the positive x direction. The carrier frequency is chosen to be in the dispersive region; $\omega_0/\omega_{pi} = 0.6$ in Fig. 3. The second trace of Fig. 3(a), show, the electron density perturbation (perturbation of the electron saturation current to a probe) detected at x = 1 cm. It indicates the same waveform as the wave excitation signal shown on the top trace. The corresponding frequency spectrum, shown in Fig. 3(b), has both upper and lower sidebands due to the amplitude modulation described by Eqs. (1) and (3). The notable features are that (i) the carrier frequency is modulated as the wave propagates. The frequency decreases at the rising part of the envelope amplitude and increases at the falling part. (ii) After the frequency modulation becomes significantly deep, so that the frequency spectra broaden [see Fig. 3(b)], each wave packet expands; the amplitude modulation disappears and frequency modulation is left at large distances. When the amplitude is small ($\delta n/n_0 \lesssim 0.001$), the frequency modulation is not observable.

The spatial evolution of carrier and sideband amplitude is shown in Fig. 4. The small-amplitude wave damps by Landau damping rate. When the initial amplitude is large, the carrier wave damps much faster than the Landau damping rate and higher-order sidebands successively grow. The curves labeled by -1, -2, -3,... indicate the amplitudes of the first, second, etc. lower sidebands appearing at the

frequencies $\omega_0-\omega_m$, $\omega_0-2\omega_m$, etc. The upper sideband amplitudes are labeled by 1, 2, ... We take notice of the fact that the nonlinear frequency modulation transfers energy between waves.

The damping rate of the total energy is much smaller than the Landau damping rate, indicating that the Landau damping disappears when the wave amplitude is large. The dips in amplitudes appearing at $x \approx 3$ cm in Fig. 4(a) are caused by the bounce oscillations of the trapped ions.[8] From the observations of the space-time evolution of a wave packet, we have confirmed that the bounce period depends on the local amplitude of the wave packet. Namely, the dip of the large amplitude part of the packet takes place at a shorter distance than the dip position of the smaller amplitude part. Although one needs to show a series of many waveform traces in order to present this feature, the upper few traces of Fig. 8 give us an indication of the effect. The flattened wave packet (2nd trace) obtained at the dip position of the large-amplitude part turns out to be peaked up at the center. This observation indicates that the trapped ion effect is localized compared to the scale-length of the wave packet. It is, of course, nonlocal over a carrier wavelength.

The energy analyzer measurements show that the trapped ion density n_T is a steep function of T_e/T_i and easily reaches $5\times10^{-3}\ n_0$, which is an appreciable fraction

of the wave density perturbation $\delta n \lesssim 0.1\, n_0$. The presence of any light-mass ions greatly enhances n_T.[9]

We now separate the amplitude $|\tilde{n}|$ and phase θ of the wave packet as

$$\tilde{n}(x,t) = |\tilde{n}| \exp(i\theta) , \qquad (4)$$

and measure θ as a function of x and t. In order to separate the slowly varying part $\exp(i\theta)$ from rapidly oscillating part $\exp(-i\omega_0 t)$ in the detected signal δn, we sample the signal at discrete times $t_\ell = (2\pi\ell/\omega_0) + t_d$, where ℓ stands for integers, and the time delay t_d is a controllable constant. We then have a signal

$$\delta n\,(x,t_\ell) = |\tilde{n}(x,t_\ell)|\, \exp[i(\theta-\omega_0 t_d+k_0 x)]. \qquad (5)$$

Note that the factor $\exp(-i\omega_0 t)$ disappears from (5).

The traces in Fig. 5 showing these sampled signals are obtained simply by imposing periodic pulsed intensity modulation on the oscilloscope traces. The intensity modulation is synchronized to the oscillator generating carrier wave signal. On the second trace obtained at x = 2 cm, we have adjusted t_d so that the phase factor in (5) equals zero at the maximum amplitude position. Because we do not have much phase shift at this small distance, the trace depicts $\delta n \simeq |\tilde{n}|$. The sampled signal $\delta n(x,t_\ell)$ oscillates at large distances. One oscillation of this signal corresponds to

a change of θ by 2π. We adjust t_d in such a way that $\theta - \omega_0 t_d + k_0 x = 2\pi(\text{integer})$ and, then, find θ from the known t_d. The measured θ is plotted in Fig. 6. The phase θ is proportional to x at given $t - x/v_g$ and has a functional form similar to the amplitude profile. We therefore express the phase as

$$\theta = \delta k(|\tilde{n}|)x. \tag{6}$$

The measurements of δk as a function of amplitude and T_e/T_i are summarized in Fig. 6. The dots, showing experimental points, indicate that $\delta k \propto |\tilde{n}|^{1/2}$ when $T_e/T_i \simeq 10$. At larger T_e/T_i, δk becomes small and dependence on $|\tilde{n}|$ deviates from square root relation. By introducing helium ions into the argon plasma we have found δk to increase. As we will discuss in Section IV, these experimental results strongly suggest that it is the trapped ions which induce the nonlinear modulation.

A single large-amplitude wave packet breaks into two wave packets as we see in Fig. 8. One of the separated wave packets has a lower carrier frequency, and propagates faster than the other one which has a higher carrier frequency. The difference of the propagation speed is large when the amplitude is large. The packet does not breakup when the amplitude is small.

III. COMPUTER SIMULATIONS

A. Model and Parameters

We have carried out numerical simulations of the experiments in order to determine the role of the trapped ions. We make use of the set of equations

$$\frac{n_e}{n_0} = \exp\left(\frac{e\varphi}{T_e}\right), \tag{7}$$

$$\frac{\partial f}{\partial t} + v\frac{\partial f}{\partial x} + \frac{eE}{M}\frac{\partial f}{\partial v} = 0, \tag{8}$$

$$-\frac{\partial^2 \varphi}{\partial x^2} = 4\pi e(n_i - n_e), \tag{9}$$

$$E = -\frac{\partial \varphi}{\partial x}. \tag{10}$$

Here, it is assumed that the electrons obey the Boltzmann distribution (7). We employ a hybrid solution algorithm originated by Denavit[10] in order to follow the ion dynamics described by (8). The simulation particles (cloud in cell model[11]) distributed on grid points (x_i, v_j) in the phase space have mass and charge which are proportional to the initial values of the distributions $f(x_i, v_j)$. The particles move along the characteristics of (8). After particles have moved, a new $f(x,v)$ is calculated from the locations and the mass of the particles. We use implicit iteration scheme[12] to find E from (7), (9), (10), and $n_i = \int dv f$. A periodic boundary condition is

imposed. We have used the total energy,

$$\varepsilon = \frac{M}{2} \int dxdv\ fv^2 + \int dx\ \left(\frac{E^2}{8\pi} + en_e\varphi \right) + \text{const}, \quad (11)$$

to check precision of computation.

The mesh sizes of grid in the phase space, Δv are chosen to be $64 < L/\Delta x < 256$ and $180 < 13v_T/\Delta v < 280$, where L is the total system length and v_T the ion thermal velocity $(T_i/M)^{1/2}$. The time step Δt is chosen to be $\omega_{pi} t = 0.2$. The distribution f is finite in a region $-5 \leq v/v_T < 8$, and is zero outside this region.

The beaming instability[13] due to the multi-stream distribution employed here is stabilized by reconstructing the distribution function before the instability grows.[10] We usually reconstruct the distribution ten times in each run.

We solve the initial value problem, in the computer simulations in constrast to the spatial wave evolution observed in the experiments. We start the simulation with the initial value

$$f(x,v) = \frac{n_0}{v_i(2\pi)^{1/2}} (1+a) \exp\left[- \frac{(v-av_p)^2}{2v_i^2} \right], \quad (12)$$

with the wave packet perturbation given by

$$a = \frac{\delta n}{n_0} = a_0 \left[1 - \varepsilon \cos (k_m x)\right] \cos (k_0 x). \qquad (13)$$

We use an approximate phase velocity v_p^2 $= (T_e/M) \left[3T_i/T_e + 1/(1+k^2\lambda_D^2)\right]$. The modulation wavenumber $k_m = (2\pi/L)$ is one-tenth of the carrier wavenumber k_0. We have tested linear dispersion relation by setting $\varepsilon = 0$ and $a = 0.001$. The result is in good agreement with linear theory.[11]

B. Results

We first show the evolution of a modulated wave in Fig. 9. The waveforms are plotted in the ion-acoustic frame, i.e., the abscissa is $x - c_s t$. The wave packet slowly moves to the left because the group velocity is smaller than c_s. In contrast to the small amplitude wave ($a_0 = 0.0025$), which only Landau damps, the large amplitude wave ($a_0 = 0.05$), shown in the left column, evolves in the following way: First of all, the amplitude becomes minimum when $\omega_{pi} t = 15$, especially at large amplitude part so that the packet flattens. The ion distribution plotted in the phase-space shows that the ions in the trapping region, $v_p - (4e|\varphi|/M)^{1/2} < v < v_p + (4e|\varphi|/M)^{1/2}$, are accelerated by the wave field and gain maximum energy when $\omega_{pi} t = 15$ (see Fig. 10). The ions almost uniformly distribute along the trajectory in the trapped region after $\omega_{pi} t = 30$. Secondly, the wavenumber modulation becomes

clear after $\omega_{pi}t = 50$. The wavenumber decreases in the front-part of the packet and increases at the packet tail. Thirdly, the wave packet flattens as the wavenumber modulation appears to be deep. All these features are exactly the same as the experimentally observed properties found in Fig. 3.

The above wavenumber modulation creates sidebands, and the wavenumber spectrum broadens as shown in Fig. 11, in contrast to the spectrum of the small amplitude wave ($a_0 = 0.0025$) which does not broaden. We already have seen the same behavior of the spectrum in Figs. 3 and 4.

We have measured the phase θ defined by (4) as a function of x, t, and the wave amplitude and have found that θ is expressed by

$$\theta = \delta\omega(|\tilde{n}|)t, \tag{14}$$

at a given $x - v_g t$. This result is obtained by assuming that the shape of $|\tilde{n}|$ does not change. The nonlinear frequency shift $\delta\omega/\omega_0$ measured when $T_e/T_i = 15$ and 20 is plotted in Fig. 7. Note that $\delta\omega$ is negative and $|\delta\omega| \propto |\tilde{n}|^{1/2}$. The value of $-\delta\omega/\omega_0$ agrees with the experimentally found $\delta k/k_0$ for the same T_e/T_i and $|\tilde{n}|$. It is a steeply decreasing function of T_e/T_i. We could barely find modulation when $T_e/T_i = 30$.

We also have obtained the nonlinear frequency shift $\delta\omega'$ of the unmodulated (monochromatic) wave from the measurements of the phase velocity $(\omega_0+\delta\omega')/k_0$. We again find that $-\delta\omega'/\omega_0$, plotted in Fig. 7, is proportional to $|\tilde{n}|^{1/2}$ and a steep function of T_e/T_i. As we will see in the next section, two frequency shifts $\delta\omega$ and $\delta\omega'$ measured by different methods are essentially the same quantity. The value of $-\delta\omega'/\omega_0$ is about 15% larger than $-\delta\omega/\omega_0$ when the amplitude is not very large. This difference between $\delta\omega$ and $\delta\omega'$ is, however, rather surprisingly small, if one thinks about the complication of trapped ion orbits in the modulated wave.

IV. ANALYSIS

A. Physical Picture and Model Equation

We have found following three features of large amplitude wave packets in both experiments and numerical simulations:

(i) The carrier frequency (wavenumber) is modulated as the wave propagates. The frequency (wavenumber) decreases at the wave packet front and increases at the tail.

(ii) The rate of modulation is proportional to $|\tilde{n}|^{1/2}$ and a steep decreasing function of T_e/T_i.

(iii) The wave packet tends to expand after above modulation becomes significantly deep.

We interpret the first feature - the modulation - as a consequence of the amplitude-dependent phase velocity. We consider a wave packet schematically depicted in Fig. 12. Suppose the phase velocity v_p of the large amplitude wave is smaller than the small-amplitude phase velocity. Then, the phase at point B in the figure moves more slowly than the phases at points A and C. As the wave propagates, the wave pattern is compressed between the points A and B and is stretched between B and C, as in the second trace. This is the modulated wave we have seen in Fig. 8. Because the wave propagates from left to right, the probe first picks up smaller wavenumber part which appears to be lower frequency part; then the larger wavenumber part, which gives rise to the higher frequency part is detected. This is the waveform shown in Figs. 3(a) and 9.

Let us analyze the above mechanism in more detail. We launch purely amplitude-modulated wave at $x = 0$. As we have found experimentally [see Eqs. (1), (4), and (6)], the wave perturbation, matching this boundary condition, is

$$a = \frac{\delta n}{n_0} = \tilde{a}(t - \frac{x}{v_g})\exp[i(k_0+\delta k)x - i\omega_0 t], \qquad (15)$$

where δk is a function of x and t through $|\tilde{a}|$. We have neglected damping. Deformation of $\tilde{a}$ is to be discussed

later. The frequency of the carrier then becomes

$$\omega = \omega_0 - x \frac{\partial \delta k}{\partial |\tilde{a}|} \frac{\partial |\tilde{a}|}{\partial t} . \qquad (16)$$

The second term gives us nonlinear frequency modulation, which is proportional to x. From $\partial \delta k / \partial |\tilde{a}| > 0$ (see Fig. 7), ω decreases when $\partial |\tilde{a}| / \partial t > 0$ and increases when $\partial |\tilde{a}| / \partial t < 0$ in agreement with the waveforms in Fig. 3. Because of $v_p = \omega_0/(k_0+\delta k)$ and $\partial \delta k / \partial |\tilde{a}| > 0$, the large-amplitude wave propagates more slowly than the small-amplitude wave, justifying physical picture shown in Fig. 12.

One can use a similar argument for the initial value problem, and find an expression,

$$a = \tilde{b}(x-v_g t)\exp[i(k_0 x-\omega_0 t-\delta\omega t)] \qquad (17)$$

which describes the wavenumber modulation appearing in the simulation.

We can easily show that (15) is a solution of

$$i\left(\frac{\partial \psi}{\partial x} + \frac{1}{v_g}\frac{\partial \psi}{\partial t}\right) = - \delta k(|\psi|)\psi \quad , \qquad (18)$$

where ψ is defined by

$$a = \psi(x,t)\exp(ik_0 x - i\omega_0 t) . \qquad (19)$$

We can also show (17) be a solution of

$$i\left(\frac{\partial\psi}{\partial t} + v_g \frac{\partial\psi}{\partial x}\right) = \delta\omega(|\psi|)\psi. \qquad (20)$$

Since the difference between (15) and (17) comes only from the boundary and initial conditions, (20) must be identical with (18), so that $\delta\omega = - v_g \delta k$. We therefore have $\delta\omega/\omega_0 = - (v_g/v_p)(\delta k/k_0) \simeq - \delta k/k_0$, because $v_g \simeq v_p$ in the ion acoustic wave. Figure 7 confirms this relation, indicating that the simulation results quantitatively agree with the experimental results except for differences appearing in a range $|\tilde{n}|/n_0 \gtrsim 0.05$.

After the carrier modulation becomes deep, so that the spectrum broadens, we need to take into account the group velocity dispersion; $v_g(k) = v_g(k_0) + \frac{1}{2}(\partial^2\omega/\partial k^2)\Delta k$, where Δk is the shift of carrier wavenumber due to the modulation. Because $\partial^2\omega/\partial k^2 < 0$ for the ion-acoustic wave, the group velocity at larger wavenumber (frequency) is smaller than v_g at smaller wavenumber. Figure 12 shows the consequence of this effect. The envelope in the region B-C of the second trace moves faster than the envelope in the part A-B where the carrier wavenumber is larger. As a result, the envelope expands and flattens as shown in the third trace. If $\partial^2\omega/\partial k^2 > 0$, although this is not the case of ion-acoustic wave, then the wave packet would shrink and peak up at the middle of the packet, i. e., one would

have a modulational instability. We now conclude that the ion-acoustic wave is stable with respect to the modulational instability.

We consider the linear dispersion relation $\omega = \omega(k)$ or $k = k(\omega)$ in order to add the above group velocity dispersion effects to our model equations (18) or (20). We have broadening in ω and k around (ω_0, k_0), because of space and time variation of $\psi(x,t)$. We write this broadening as $k = k_0 + \Delta k$ and $\omega = \omega_0 + \Delta\omega$ and expand k in a series of $\Delta\omega$ up to $\Delta\omega^2$. Using $k_0 = k(\omega_0)$, $\Delta\omega\psi = i\partial\psi/\partial t$, and $\Delta k\psi = - i\partial\psi/\partial x$, we find

$$\frac{\partial\psi}{\partial x} + \frac{1}{v_g}\frac{\partial\psi}{\partial t} - \frac{1}{2}\frac{\partial^2 k}{\partial\omega^2}\frac{\partial^2\psi}{\partial t^2} = 0. \qquad (21)$$

The last term of (21) represents the modification of wave packet due to the above mentioned group velocity dispersion. We replace left-hand-side of (18) by (21) and obtain

$$i\left(\frac{\partial\psi}{\partial x} + \frac{1}{v_g}\frac{\partial\psi}{\partial t}\right) + p\frac{\partial^2\psi}{\partial t^2} + \delta k(|\psi|)\psi = 0, \qquad (22)$$

where,

$$p = - \frac{1}{2}\frac{\partial^2 k}{\partial\omega^2} = \frac{1}{2}\frac{1}{v_g^3}\frac{\partial^2\omega}{\partial k^2} \quad .$$

We also obtain

$$i\left(\frac{\partial\psi}{\partial t} + v_g \frac{\partial\psi}{\partial x}\right) + \alpha \frac{\partial^2\psi}{\partial x^2} - \delta\omega(|\psi|)\psi = 0, \qquad (23)$$

with

$$\alpha = \frac{1}{2}\frac{\partial^2\omega}{\partial k^2} = -v_g^3 p \quad \text{and} \quad \delta\omega = -v_g \delta k$$

in the same manner. The transformation,

$$s = t - \frac{x}{v_g}, \qquad \xi = x, \qquad (24)$$

yields (22) to be

$$i\frac{\partial\psi}{\partial\xi} + p\frac{\partial^2\psi}{\partial s^2} + \delta k\psi = 0, \qquad (25)$$

and

$$y = x - v_g t, \qquad \tau = t \qquad (26)$$

yields (23) to be

$$i\frac{\partial\psi}{\partial t} + \alpha\frac{\partial^2\psi}{\partial y^2} - \delta\omega\psi = 0. \qquad (27)$$

The nonlinear Schrödinger equations (25) or (27) are now supposed to describe the observed wave evolution provided the nonlinear coefficients δk and $\delta\omega$ have functional forms given in Fig. 7. When $|\psi|$ is not very large and $T_e/T_i \lesssim 30$, we have found that $\delta k \propto -\delta\omega \propto |\psi|^{1/2}$. Equation (25) is suitable for analyzing the boundary value problem, and (27) for the initial value problem.

B. Trapped-Ion Effects

Before studying the properties of (25) and (27), we need to discuss the principal process causing the nonlinear frequency or wavenumber shift. The dependence $\delta k \propto |\psi|^{1/2}$ strongly suggests that the particles trapped in the troughs of wave potential play an important role. The fact that δk is a steeply decreasing function of $T_e/T_i [= (\omega/kv_i)^{1/2}]$ indicates that the trapped-ions are the source of nonlinear effects, because the density of trapped ions is a steeply decreasing function of ω/kv_i. Because v_p is not much different from v_g in the case of the ion-acoustic wave, the lifetime of the potential troughs is much longer than the ion bounce time $\tau_B \equiv (M/|e\varphi|k_0^2)^{1/2}$ under our experimental parameters. We have found by the simulation that each period of the carrier wave reach a nearly local equilibrium state by trapping ions after an initial amplitude oscillation.

Several authors[14-17] have calculated the nonlinear frequency shift $\delta\omega$ due to trapped electrons to discuss nonlinear electron plasma waves. We use their result to estimate $\delta\omega$ for the ion-acoustic wave due to trapped ions by simply replacing the electron distribution by the ion distribution and introducing ion contribution to the dielectric function. We then have

$$\frac{\delta k}{k_0} = -\frac{\delta\omega}{v_g\omega_0} \simeq \frac{\Gamma v_p^3 c_s}{v_g} f_0''(v_p)|\psi|^{1/2} , \qquad (28)$$

where $f_0''(v_p)$ is the second derivative of the ion velocity distribution evaluated at $v = v_p$, $c_s = (T_e/M)^{1/2}$, and $|\psi| = |\tilde{n}|/n_0$. The numerical factor Γ, which depends on the method of calculation[14-17] and has values $0.7 < \Gamma < 1.8$, is here choosen to be $\Gamma = 1$. We also set $v_g = v_p = c_s$ and plot (28) in Fig. 7 for a few different values of T_e/T_i. The theoretical prediction (28), made for monochromatic wave, agrees with experimental and computational results which are measured for both modulated and monochromatic waves, indicating that one can treat the phase velocity shift due to the trapped particles as a local effect as long as the scale length of the wave packet is much longer than the carrier wavelength.

We should note that Eq. (28) is obtained by expanding the velocity distribution in a series of $v_{tr}v_p/v_i^2$, where v_{tr} is the trapping velocity $(4e\phi/M)^{1/2}$. Therefore, (28) is only valid when $|\psi| = |\tilde{n}|/n_0 < (T_i/T_e)^2$, which is a range below the experimental and computational amplitude level. It is surprising that all frequency or wavenumber shifts, found in the experiments[18-20] and simulations[21] of the monochromatic ion acoustic and

electron plasma waves, including our results, agree with (28) even when $v_{tr}v_p/v_i^2 \gtrsim 1$.

Recently Kim[22] has calculated $\delta\omega$ to a higher order of $v_{tr}v_p/v_i^2$. He has found that $\delta\omega$ decreases and changes sign at large amplitude. This zero crossing of $\delta\omega$ is found in our simulations of the monochromatic waves when $T_e/T_i = 30$ (see Fig. 6). In contrast to theory and simulations, our experimental results and the results of the electron plasma wave experiments obtained by Vidmar, Malmberg and Starke[19] indicate that $\delta k/k_0$ increases more rapidly than $\delta k \propto |\psi|^{1/2}$ for larger amplitudes.

We now discuss the behavior of the trapped ions in further detail by considering ion orbits in the phase space depicted in Fig. 13. If the ions are deeply trapped, namely the ion distribution f is large in the region A in the phase space, then the trapped ion density is high at the bottom of the potential trough. In comparison with linear theory, these bunched ions weaken the wave field and decrease the phase velocity so that one has $\delta\omega < 0$. In contrast the marginally trapped ions in the region B stay longer at the top of the potential, strengthen the wave field, and cause positive $\delta\omega$. The width of the region B must be very narrow, because even the trapped ion distribution plotted in Fig. 10 bring about negative $\delta\omega$. We are now able to account for zero crossing of $\delta\omega$. The

marginally trapped ions can be created, when both T_e/T_i and ψ are large, so that v_p/v_i and v_{tr}/v_i are large, because the lower velocity end of the trapping region reaches the steep Maxwellian tail of the ion distribution as shown in Fig. 13. If v_p/v_i or v_{tr}/v_i or both are small, then deeply trapped ions are created.

Because the velocity width, Δv, of the marginally trapped distribution is very small compared to the thermal velocity, the ion-ion collisions easily destroy such a narrow distribution.[23] If we employ the Fokker-Planck model

$$\frac{df}{dt} = \nu_{ii} \frac{\partial}{\partial v} \left(vf + \frac{v_i^2}{2} \frac{\partial f}{\partial v} \right) , \qquad (29)$$

then the life time of the distribution becomes $\tau_t \sim 2(\Delta v/v_i)^2 \nu_{ii}^{-1}$. From the simulation results, we estimate $\Delta v/v_i$ to be about 0.2. Now τ_t becomes only 10 μsec which is shorter than the ion bounce time. We therefore conclude that the narrow distributions causing positive $\delta\omega$ can rarely be formed. The discrepancy between experimental and simulation results arise from the fact that the simulations are based on the Vlasov model.

We note here that the nonlinear term associated with wave-wave coupling[3,4] is estimated to be more than an order of magnitude smaller than observed $|\delta k|$ or $|\delta\omega|$ at $T_e/T_i = 30$ when $|\psi| \lesssim 0.1$. The trapped electron

effect,[24] which was considered to turn δk to be negative, did not appear.

C. Numerical Solutions of Model Equation

To test how well our model equation describes the observed wave evolution, we solve (28) numerically. We employ an approximate wavenumber shift

$$\delta k = q|\psi|^{1/2} \quad , \tag{30}$$

and use the boundary condition (3). In Fig. 14, we show the spatial evolution of the amplitude $|\psi|$ and the phase θ. The numerical values of parameters are given in the caption. The phase is expressed by $\theta = q|\psi|^{1/2}x$ and $|\psi|$ does not change much when the distance x is small. The amplitude tends to flatten at large x. All these features are consistent with our observations.

A discrepancy appears in the evolution of the phase occurring around the minimum amplitude point in the boundary value. In contrast to the experimental waveform developing a frequency jump (a jump of $-\partial\theta/\partial t$) [see the bottom trace of Fig. 3(a)], the phase found in the numerical solution becomes smooth at large x by emitting two solitons. We should note that our model equation is not valid when (i) the amplitude is too small to have trapped ions within the experimental extent of time, and when (ii) the variation of envelope $(\partial\psi/\partial y)/\psi$ is comparable to the carrier wavenumber k_0, because the trapped ion effects are nonlocal over a carrier wavelength.

D. Wave Packet Breaking

We now discuss the properties of (27), which is related to the wave packet breaking shown in Fig. 8. We employ an approximate frequency shift

$$\delta\omega = \beta|\psi|^{1/2} \quad . \tag{31}$$

Following Ref. 25, we write ψ in the form

$$\psi = \rho^{\frac{1}{2}} \exp\left(i\int \frac{\sigma dy}{2\alpha}\right), \tag{32}$$

where ρ and σ are real functions of y and τ. We substitute (31) and (32) into (27) and obtain

$$\frac{\partial\rho}{\partial\tau} + \frac{\partial}{\partial y}(\rho\sigma) = 0, \tag{33}$$

and

$$\frac{\partial\sigma}{\partial\tau} + \sigma\frac{\partial\sigma}{\partial y} = -2\alpha\beta\rho^{-\frac{3}{4}}\frac{\partial\rho}{\partial y} + \alpha^2\frac{\partial}{\partial y}\left[\rho^{-\frac{1}{2}}\frac{\partial}{\partial y}\left(\rho^{-\frac{1}{2}}\frac{\partial\rho}{\partial y}\right)\right] . \tag{34}$$

The set of equations (33) and (34) is very similar to the set of hydrodynamic equations if one replaces ρ and σ by the density and the velocity of fluid. Therefore one may use the arguments of the one-dimensional gas dynamics.[26]

We first consider a slowly varying waveform, so that the last term in (34) can be neglected. We, then, immediately find that the sign of $\alpha\beta$ corresponds to the

sign of "temperature". If $\alpha\beta < 0$, then we have negative "temperature" system, meaning that the wave packet is unstable. Our observations indicate that $\alpha < 0$ and $\beta < 0$, so that $\alpha\beta > 0$.

One may easily find the Riemann invariants

$$J_{\pm} = \sigma \pm 8(2\alpha\beta\rho^{\frac{1}{4}})^{1/2} \tag{35}$$

to satisfy

$$\left\{ \frac{\partial}{\partial\tau} + [\sigma \pm (2\alpha\beta\rho^{\frac{1}{4}})^{1/2}] \frac{\partial}{\partial y} \right\} J_{\pm} = 0. \tag{36}$$

The perturbations propagate along the characteristics defined by

$$\frac{dy}{d\tau} = \sigma \pm (2\alpha\beta\rho^{\frac{1}{4}})^{1/2} . \tag{37}$$

The breaking of the wave packet shown in Fig. 8 corresponds physically to the expansion of gas into a vacuum. Figure 15 illustrates the evolution of ρ following (33) and (34). The characteristics c_1 and c_2 have positive sign and c_3 and c_4 have negative sign in (37). Note that c_1 and c_4 indicate trajectories of compression front and c_2 and c_3 show rarefaction trajectories. We find that a single humped ρ profile breaks into a double hump. The relative velocity of separated packets is mainly given by the difference in σ. The large amplitude wave attains large σ, which is proportional to the wavenumber modulation, in

a short time. The packet moving in the positive y-direction has $\sigma > 0$ and the one in the negative direction has $\sigma < 0$. The second term of (37) has a weak dependence on ρ.

We find from (36) that the small perturbations around $\sigma = 0$ and $\rho = \rho_0 = \text{const.}$ propagate in both positive and negative y-directions with the velocity $u_\pm = \pm (2\alpha\beta\rho_0^{\frac{1}{4}})^{1/2}$. Taking the third order derivative term in (34) into account and following the prescription described in Ref. 25, we obtain the Korteweg-deVries equation

$$\frac{\partial\tilde{\rho}}{\partial\tau} + u_\pm \frac{\partial\tilde{\rho}}{\partial y} - \frac{15u_\pm}{8\rho_0}\tilde{\rho}\frac{\partial\tilde{\rho}}{\partial y} + \frac{\alpha^2}{2u_\pm}\frac{\partial^3\tilde{\rho}}{2y^3} = 0, \qquad (38)$$

which describes the evolution of perturbation $\tilde{\rho} = \rho - \rho_0$. This equation predicts envelope steepening and the formation of "dark" envelope solitons (the amplitude decreases at the soliton position).[27] One also can derive stationary soliton solution directly from (27) and (30). We can observe the soliton formation in our experimental extent of time ($\sim 200\ \omega_0^{-1}$) if we choose proper initial conditions. The details of the experimental observation of solitons are to be described in a forthcoming publication.

V. CONCLUSIONS

We have found experimentally the following features of large amplitude ion-acoustic wave packet:

(i) The amplitude modulated waves develope self-frequency or wavenumber modulation.

(ii) The self-modulation together with the dispersion effect causes the wave packet to expand and to break into two packets. The ion-acoustic wave is stable with respect to the modulational instability.

(iii) The self-modulation is proportional to the square root of the wave amplitude and is a steep function of the electron to ion temperature ratio, indicating that the trapped ions play a crucial role.

(iv) The wave-wave coupling process discussed in the most theoretical papers turns out to be minor effect. Our computer simulation has reproduced all above experimentally found features. It discloses existence of trapped ions when the self-modulation appears. We have shown that the combination of amplitude-dependent phase velocity and group velocity dispersion accounts for the wave evolution. We have phenomenologically derived a model equation, which takes into account both trapped ion and dispersion effects. The model equation accounts for the wave packet breaking and suggests that ion-acoustic dark solitons will be formed.

ACKNOWLEDGMENTS

The authors wish to thank R. A. Stern for use of his experimental facility and N. L. Schryer for use of his computer

program for solving the nonlinear Schrödinger equation. They appreciate helpful conversations with T. K. Chu, Y. H. Ichikawa, A. Hasegawa, K. Mima, K. Nishikawa, T. Taniuti, and F. D. Tappert.

REFERENCES

1. B. B. Kadomtsev, and V. I. Karpman, Usp. Fiz. Nauk 103, 193 (1970). [Sov. Phys. USPEKHI 14, 40 (1971)]; T. Taniuti et al. Prog. Theor. Phys. Supplement No. 55 (1974).
2. Y. H. Ichikawa, and T. Taniuti, J. Phys. Soc. Japan 34, 513 (1973).
3. Y. H. Ichikawa, T. Imamura, and T. Taniuti, J. Phys. Soc. Japan 33, 189 (1972).
4. T. Kakutani, and N. Sugimoto, Phys. Fluids 12, 1617 (1974).
5. R. J. Taylor, K. R. MacKenzie, and H. Ikezi, Rev. Sci. Instr. 43, 1675 (1972).
6. H. Ikezi, K. Mima, K. Nishikawa, and M. Inutake, Phys. Rev. Lett. 36, 794 (1976).
7. B. D. Fried and R. W. Gould, Phys. Fluids 4, 139 (1960).
8. T. M. O'Neil, Phys. Fluids 8, 2255 (1965); L. M. Al'tsul, and V. I. Karpman, Sov. Phys. JETP 22, 361 (1966); J. H. Malmberg and C. B. Wharton, Phys. Rev. Lett. 19, 775 (1967); H. Ikezi, Y. Kiwamoto, K. Nishikawa, and K. Mima, Phys. Fluids 15, 1605 (1972).
9. I. Alexeff, W. D. Jones, and D. Montgomery, Phys. Rev. Lett. 19, 422 (1967).
10. J. Denavit, J. Comput. Phys. 9, 75 (1972).
11. A. B. Langdon, J. Comput. Phys. 6, 247 (1970).
12. P. H. Sakanaka, C. K. Chu, and T. C. Marshall, Phys. Fluids 14, 611 (1971).
13. J. M. Dawson, Phys. Rev. 118, 381 (1960).

14. W. M. Manheimer, and R. W. Flynn, Phys. Fluids 14, 2393 (1971).

15. R. L. Dewar, Phys. Fluids 15, 712 (1972).

16. G. J. Morales, and T. M. O'Neil, Phys. Rev. Lett. 28, 417 (1972).

17. A. Lee and G. Pocobelli, Phys. Fluids 15, 2351 (1972).

18. H. Sugai and E. Märk, Phys. Rev. Lett. 20, 127 (1975).

19. P. J. Vidmar, J. H. Malmberg, and T. P. Starke, Phys. Fluids, 19, 32 (1976).

20. H. Sugai, R. Hatakeyama, K Saeki,and M. Inutake, Phys. Fluids 19, 1753 (1976).

21. Y. Matsuda and F. W. Crawford, Phys. Fluids, 18, 1336 (1975).

22. H. Kim, Phys. Fluids 19, 1362 (1976).

23. H. Ikezi, N. Takahashi and K. Nishikawa, Phys. Fluids 12, 853 (1968); A. Y. Wong, and D. R. Baker, Phys. Rev. 188 326 (1969).

24. R. L. Dewar, W. L. Kruer and W. M. Manheimer, Phys. Rev. Lett. 28, 215 (1972).

25. T. Taniuti and N. Yajima, J. Math. Phys. 10, 1369 (1969).

26. L. D. Landau and E. M. Lifshitz, Fluid Mechanics, (Pergamon Press, 1959) Chap. 10.

27. A. Hasegawa, Plasma Instabilities and Nonlinear Effects, (Springer-Verlag, 1975) p. 200.

FIGURE CAPTIONS

Fig. 1 Electron density perturbation versus time, showing propagation of small amplitude wave packet at various carrier wave frequencies ω_0. The wave signals are detected at x = 8 cm. The wave excitation signal, only for $\omega_0/2\pi$ = 0.4 MHz is shown. The wave packet shape of the excitation signal is kept unchanged.

Fig. 2 Schematic of experimental device and Langmuir probe curves showing change of T_e.

Fig. 3 (a) Electron density perturbation versus time with distance from the wave excitation points x as a parameter. Arrows indicate delay of signal due to wave packet propagation.
(b) Frequency spectra of the waves shown in (a).

Fig. 4 Spatial amplitude variation of carrier and side-bands. m indicates component at the frequency $\omega_0 + m\omega_m$. (a) Large amplitude case. (b) Small amplitude case.

Fig. 5 Sampled signal $\delta n(t = 2\pi \ell /\omega_0)$ showing phase shift in $\tilde{n}$. $\omega_0/2\pi$ = 400 KHz, $\omega_{pi}/2\pi \simeq$ 1 MHz, T_e/T_i = 13, k_0 = 15 cm^{-1}.

Fig. 6 The envelope amplitude $|\tilde{n}|$ and phase θ as a function of time $t - (x/v_g)$ with the distance x as a parameter. $\omega_0/2\pi$ = 400 KHz, $\omega_{pi}/2\pi$ = 1 MHz, T_e/T_i = 13, k_0 = 15 cm^{-1}.

Fig. 7 Nonlinear wavenumber shift $\delta k/k_0$ (experimental and theoretical) and frequency shift $-\delta\omega/\omega_0$ (simulation) as a function of $(|\tilde{n}|/n_0)^{1/2}$. Dots are experimental points; circles and triangles the simulation results for modulated and monochromatic waves. Solid lines show Eq. (28). The ends of solid lines indicate $v_{tr}v_p/v_i = 1$.

Fig. 8 Wave perturbation versus $(x/v_g) - t$ with distance as a parameter. $\omega_0/2\pi$ = 500 KHz, $\omega_{pi}/2\pi \simeq$ 1 MHz, $T_e/T_i \simeq 15$, c_s = 1.7×10^5 cm/sec.

Fig. 9 Evolution of periodically modulated wave obtained by computer simulation. Two modulation periods are plotted in the ion acoustic frame. $k_0/k_D = 1$, $T_e/T_i = 20$. (a) $a_0 = 0.05$, $\varepsilon = 1$ [see Eq. (13)]. (b) $a_0 = 0.0025$, $\varepsilon = 1$.

Fig. 10 The ion distribution, f, in the phase space. The equi-f contours are plotted. The contours are defined by $\log(f/f_{max}) = 0.24j$, where j = 0,1,...,10, and f_{max} is the maximum value of unperturbed distribution. The bottom curve in each diagram indicates $f = f_{max}$ and the top trace shows $f = 0.004\ f_{max}$. The parameters are the same as those in the case of Fig. 9. Two packet periods are plotted.

Fig. 11 The wave number spectra. The parameters in (a) and (b) are the same as those in the case of Fig. 9(a) and (b) respectively.

Fig. 12 Schematic of wave evolution.

Fig. 13 The relation between wave potential, trapping region in phase space and ion distribution.

Fig. 14 Numerical solution of Eq. (25). $q = 0.1$ ($T_e/T_i = 15$). $\omega_0/\omega_{pi} = 0.45$, $\omega_m/\omega_0 = 1/15$.

Fig. 15 Characteristics and amplitude profile in y-τ plane.

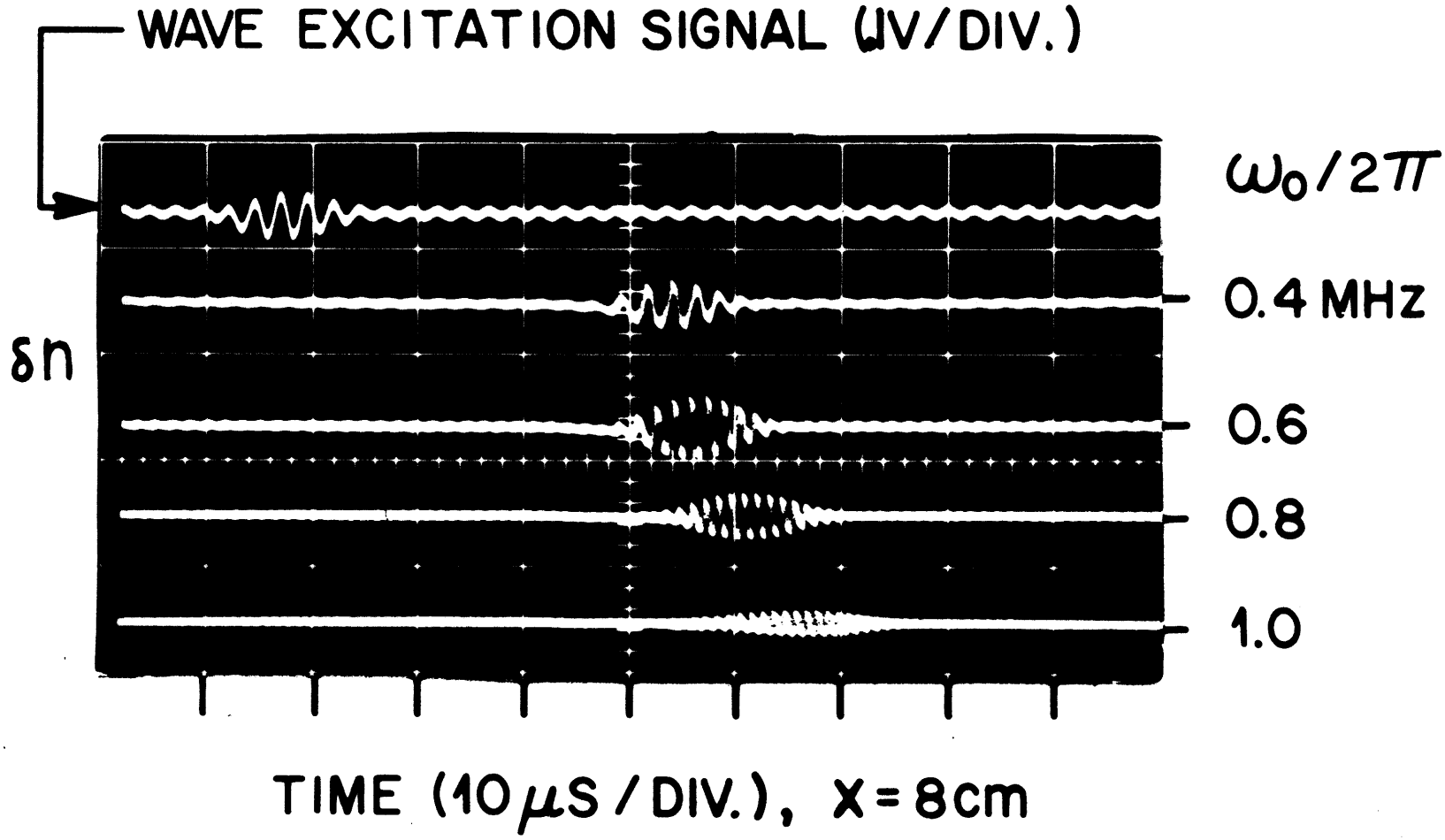
WAVE EXCITATION SIGNAL (μV/DIV.)
δn
ω0/2π
0.4 MHz
0.6
0.8
1.0
TIME (10 μS / DIV.), X = 8cm

Figure 1

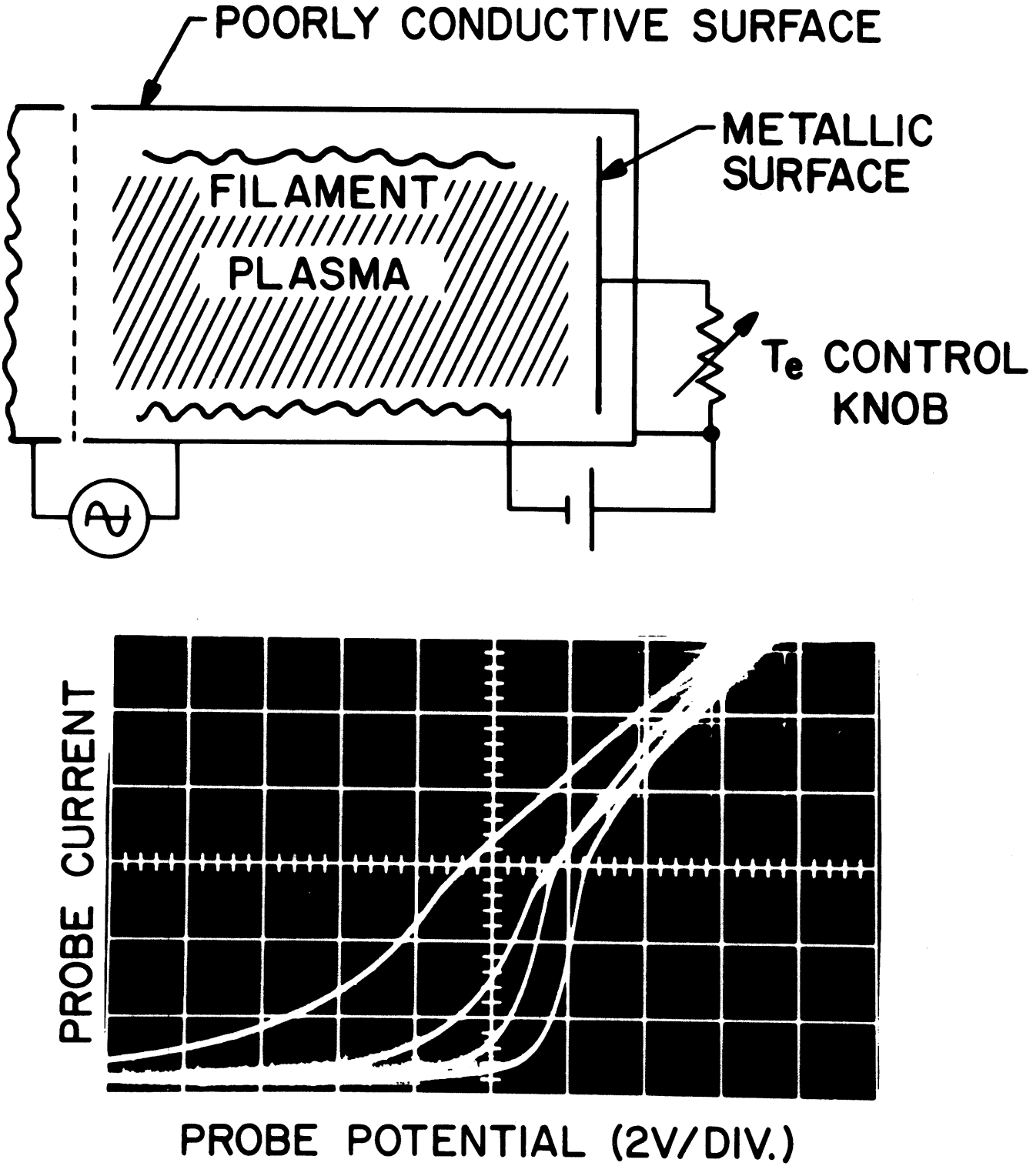
POORLY CONDUCTIVE SURFACE
METALLIC SURFACE
FILAMENT
PLASMA
T_e CONTROL KNOB
PROBE CURRENT
PROBE POTENTIAL (2V/DIV.)

Figure 2

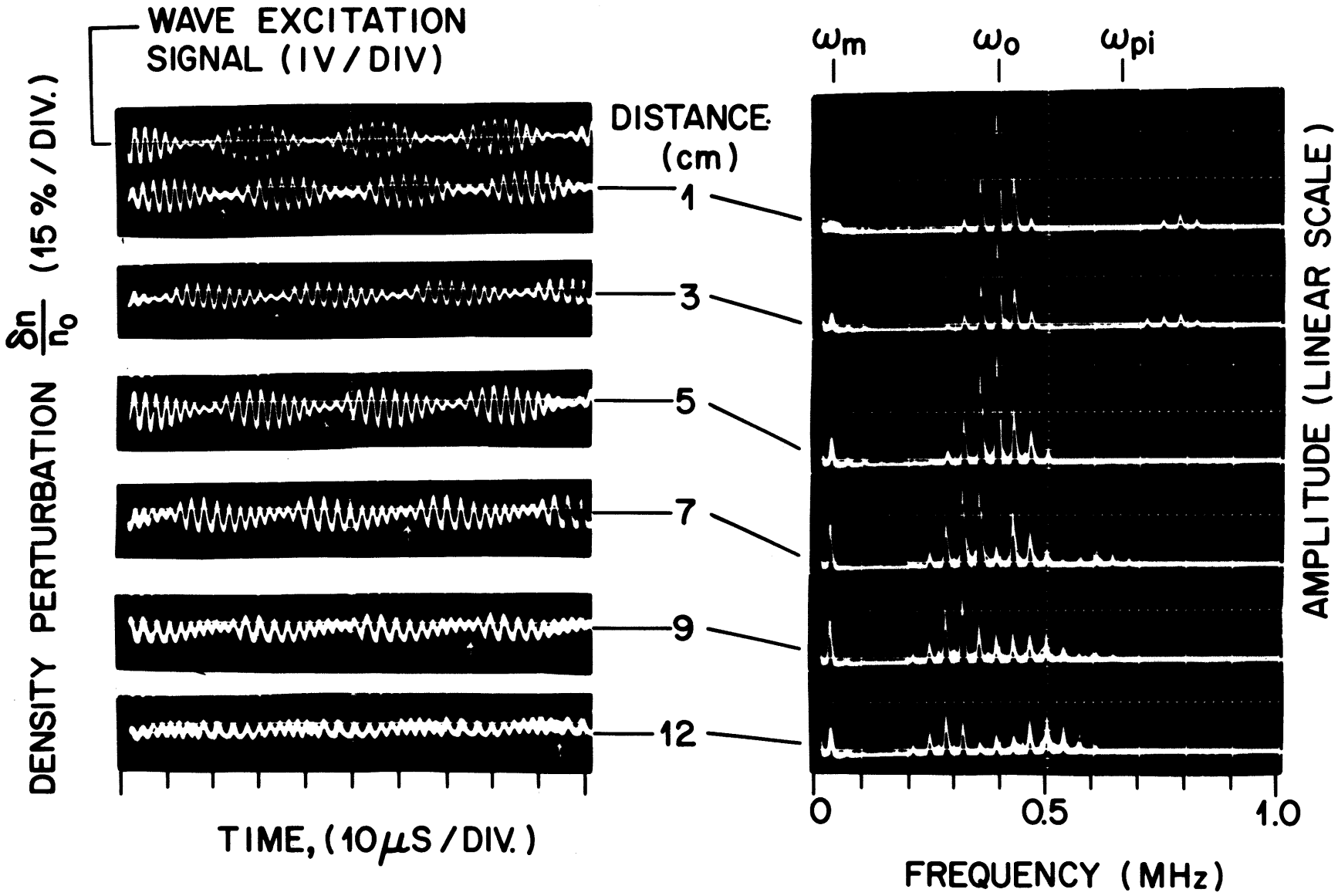
WAVE EXCITATION
SIGNAL (1V/DIV)
DISTANCE (cm)
1
3
5
7
9
12
$\frac{\delta n}{n_o}$ (15 % / DIV.)
DENSITY PERTURBATION
TIME, (10μS / DIV.)
ω_m
ω_o
ω_{pi}
0
0.5
1.0
FREQUENCY (MHz)
AMPLITUDE (LINEAR SCALE)

Figure 3

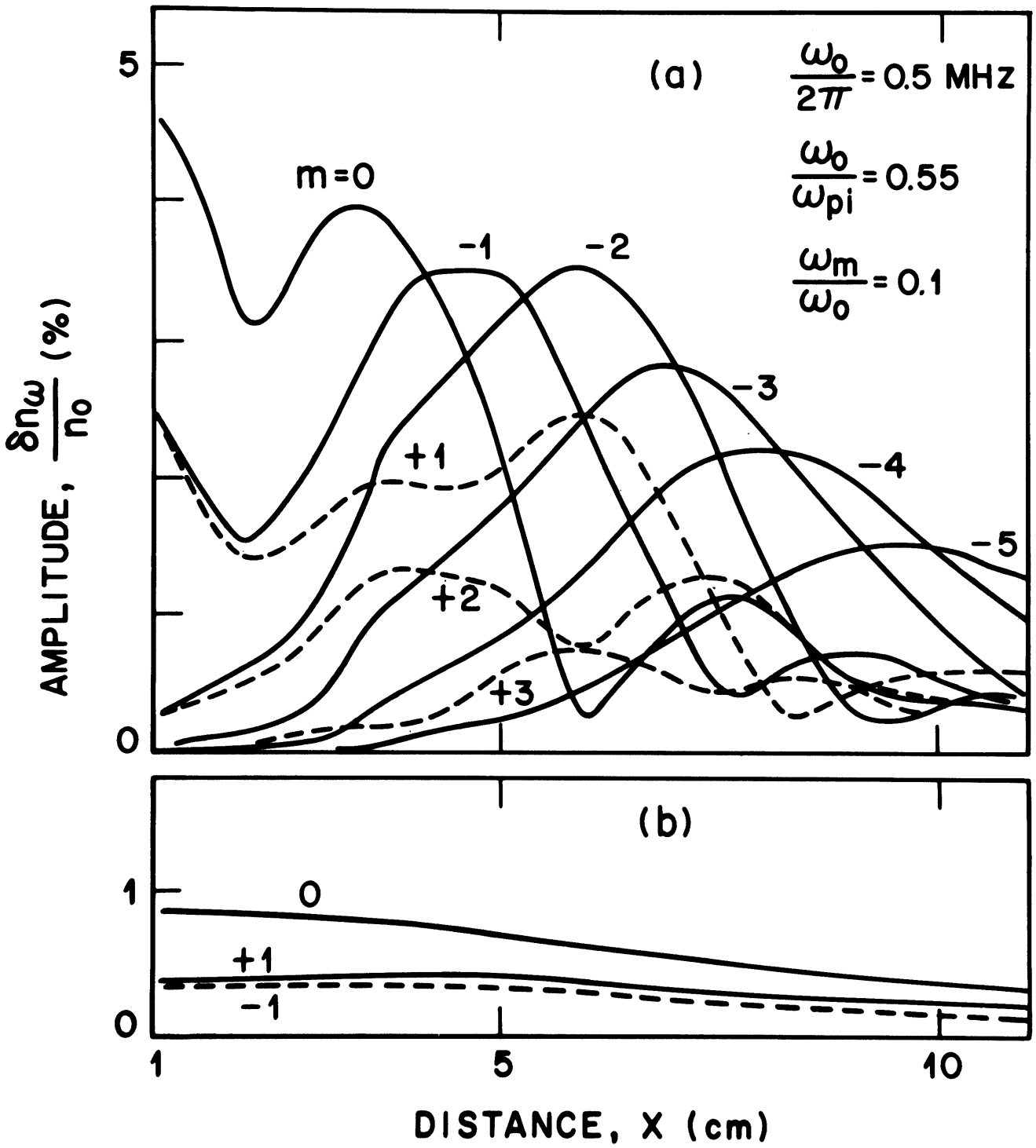
(a)
$\frac{\omega_0}{2\pi}$ = 0.5 MHz
$\frac{\omega_0}{\omega_{pi}}$ = 0.55
$\frac{\omega_m}{\omega_0}$ = 0.1
m=0
-1
-2
-3
-4
-5
+1
+2
+3
5
0
AMPLITUDE, $\frac{\delta n_\omega}{n_0}$ (%)
(b)
0
+1
-1
1
0
1
5
10
DISTANCE, X (cm)

Figure 4

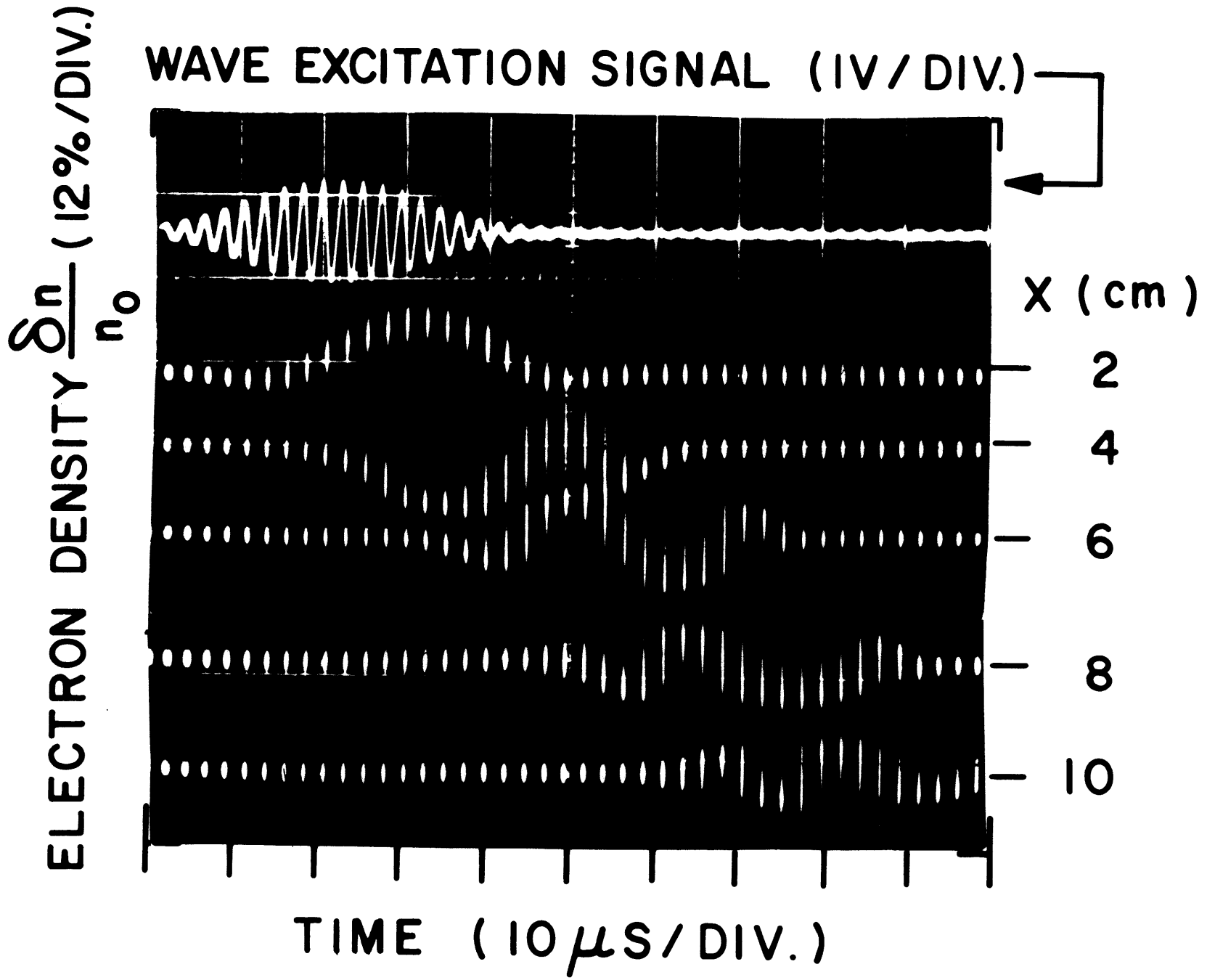
WAVE EXCITATION SIGNAL (IV/DIV.)
ELECTRON DENSITY $\frac{\delta n}{n_o}$ (12%/DIV.)
X (cm)
2
4
6
8
10
TIME (10 μS/DIV.)

Figure 5

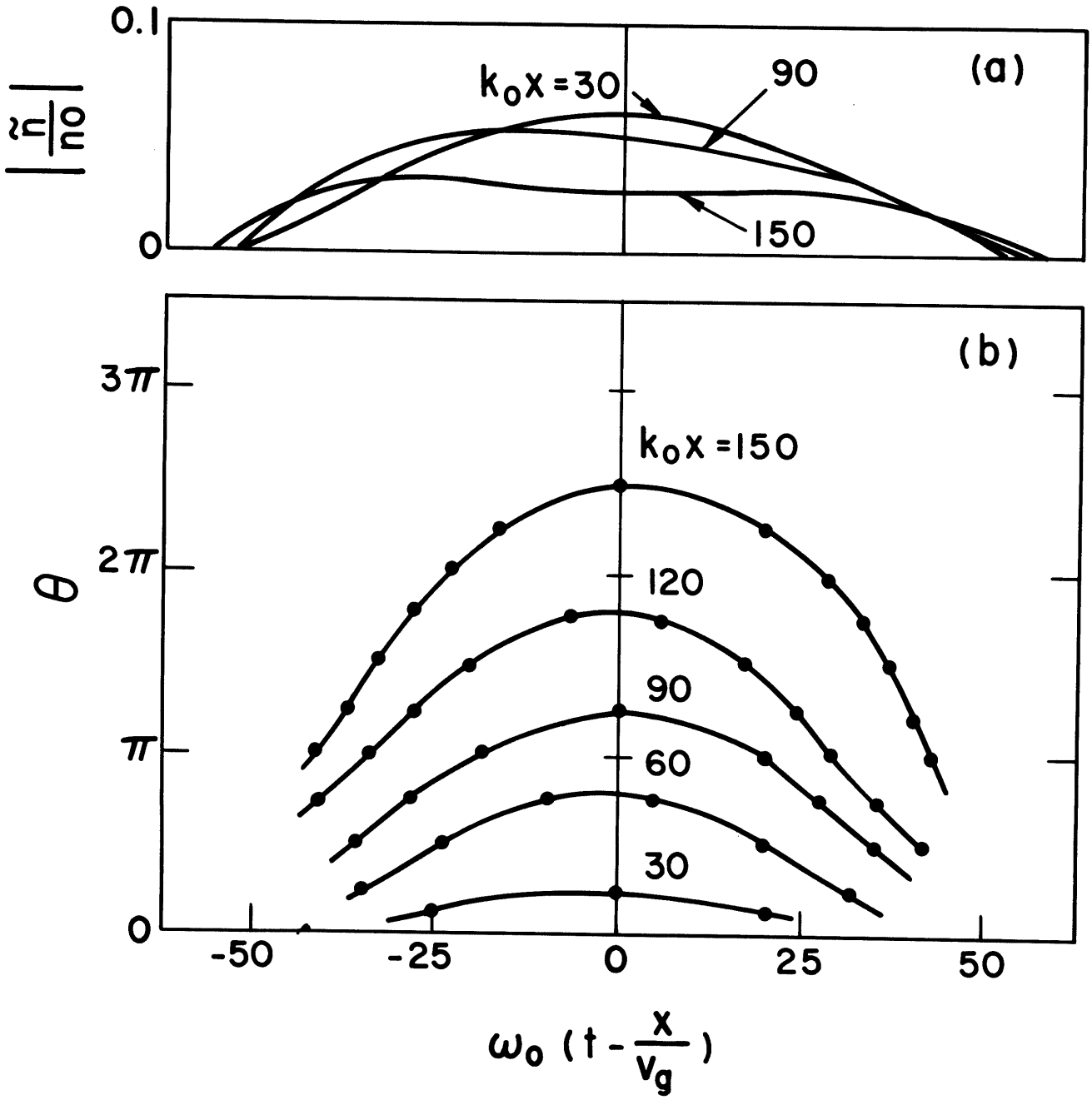
0.1
0
$\frac{|n|}{n_0}$
$k_0x=30$
90
150
(a)
(b)
3π
2π
π
0
θ
$k_0x=150$
120
90
60
30
-50
-25
0
25
50
$\omega_0\left(t-\frac{x}{v_g}\right)$

Figure 6

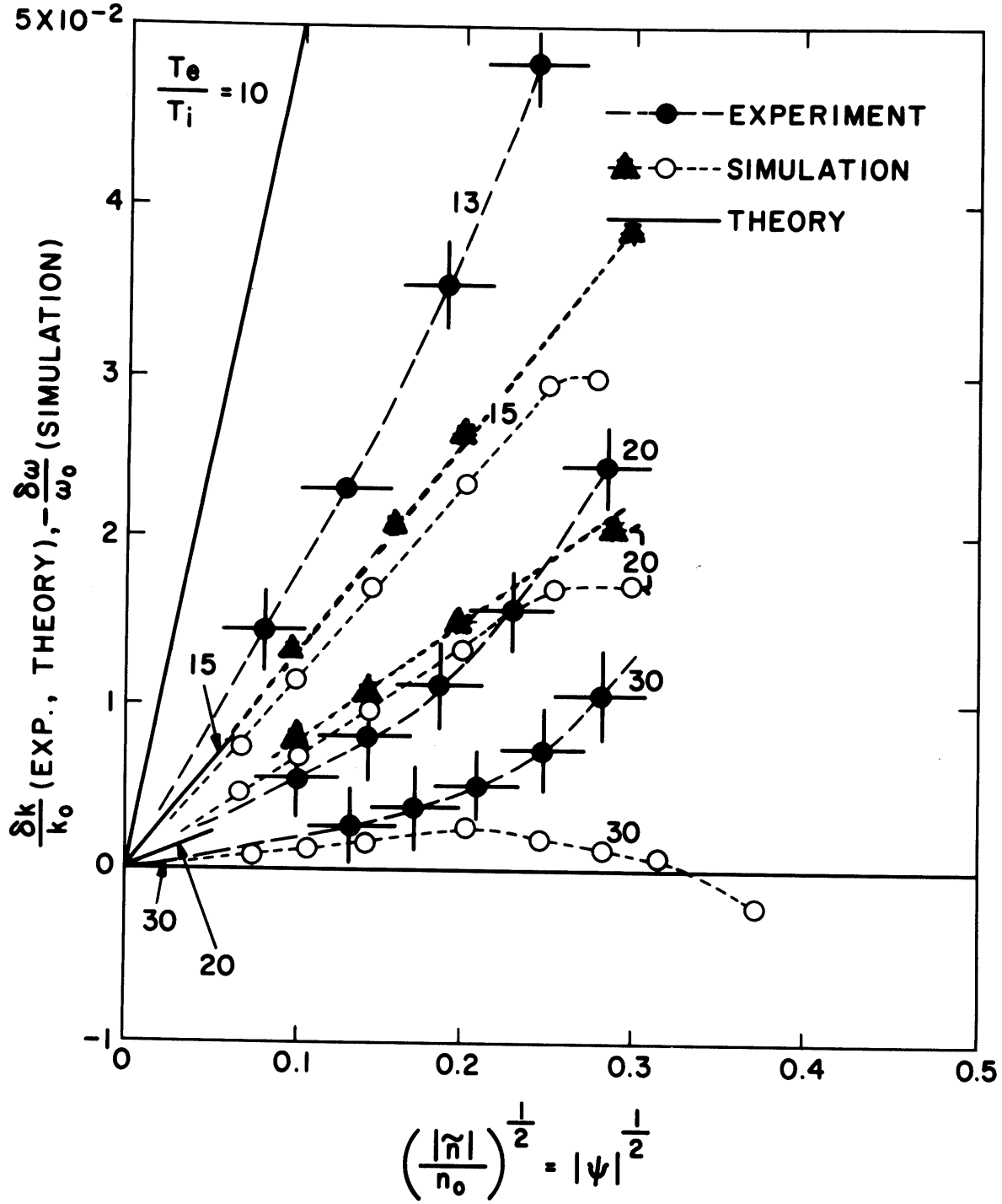
5X10⁻²
Te/Ti = 10
EXPERIMENT
SIMULATION
THEORY
13
15
20
20
15
30
30
20
30
4
3
2
1
0
-1
0
0.1
0.2
0.3
0.4
0.5
δk/k₀ (EXP., THEORY), -δω/ω₀ (SIMULATION)
(|ñ|/n₀)^½ = |ψ|^½

Figure 7

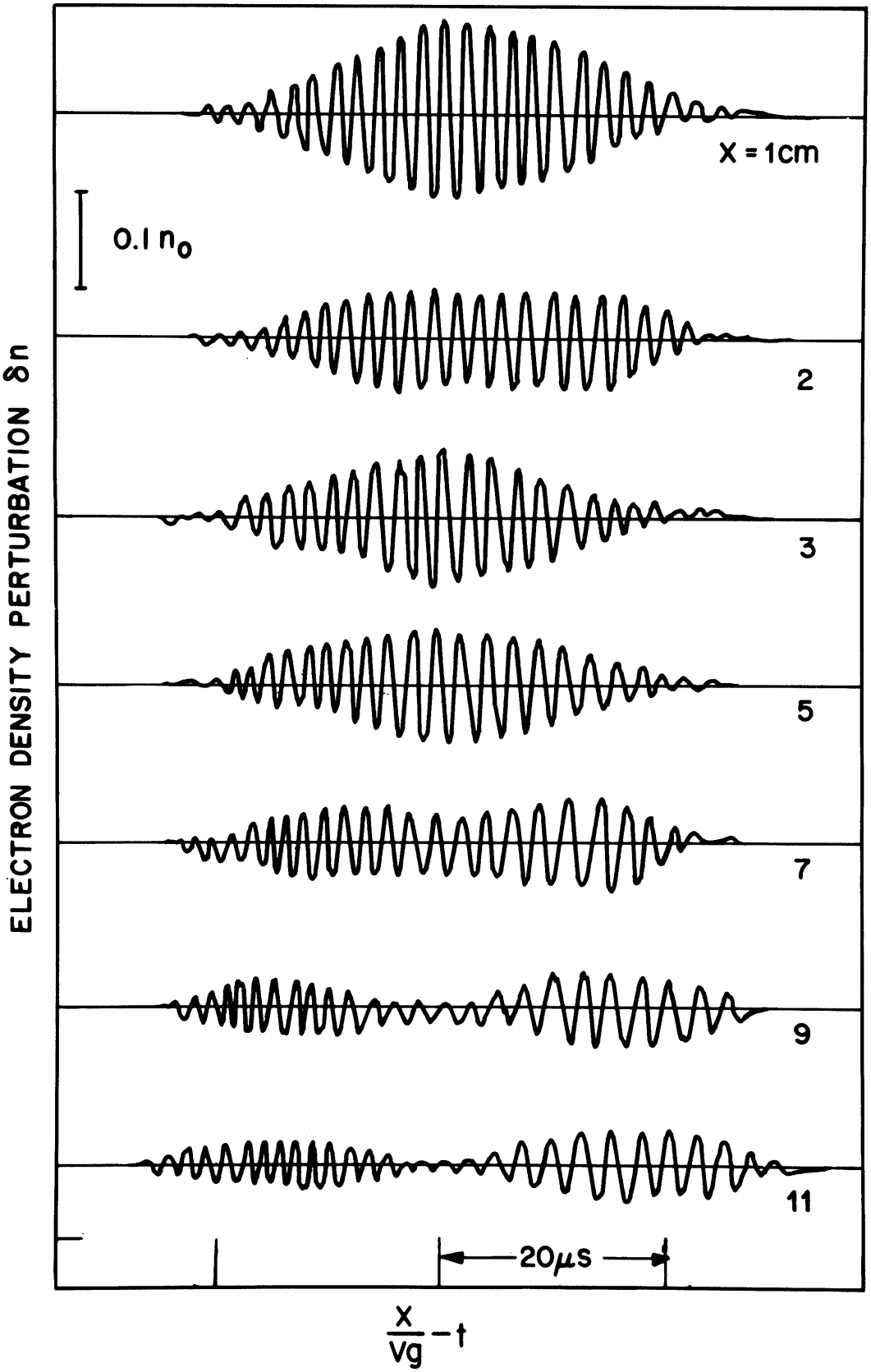
ELECTRON DENSITY PERTURBATION δn
X = 1cm
0.1 n0
2
3
5
7
9
11
20μs
X/Vg − t

Figure 8

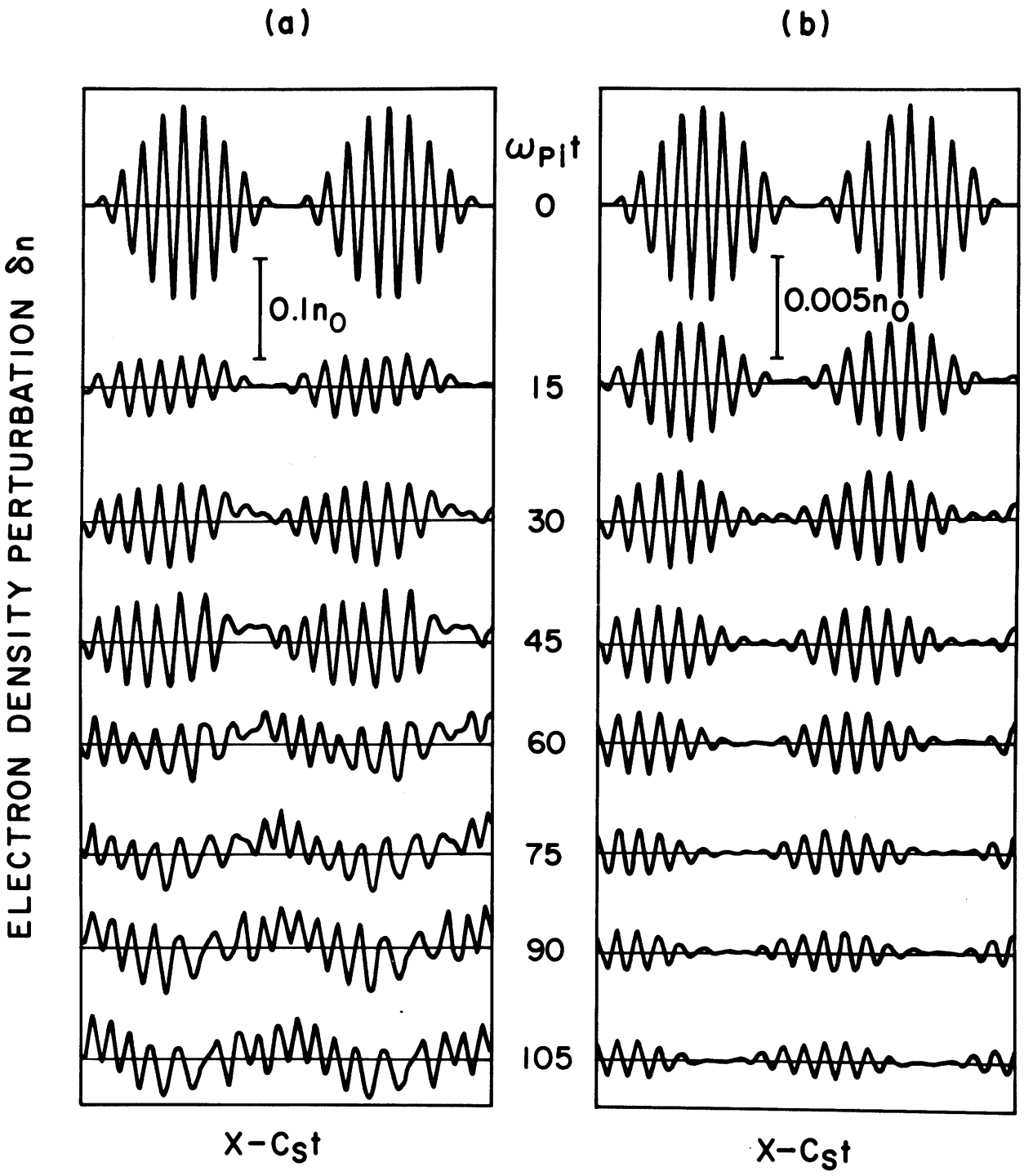
(a)
(b)
ELECTRON DENSITY PERTURBATION δn
ωPit
0
15
30
45
60
75
90
105
0.1n0
0.005n0
X-Cst
X-Cst

Figure 9

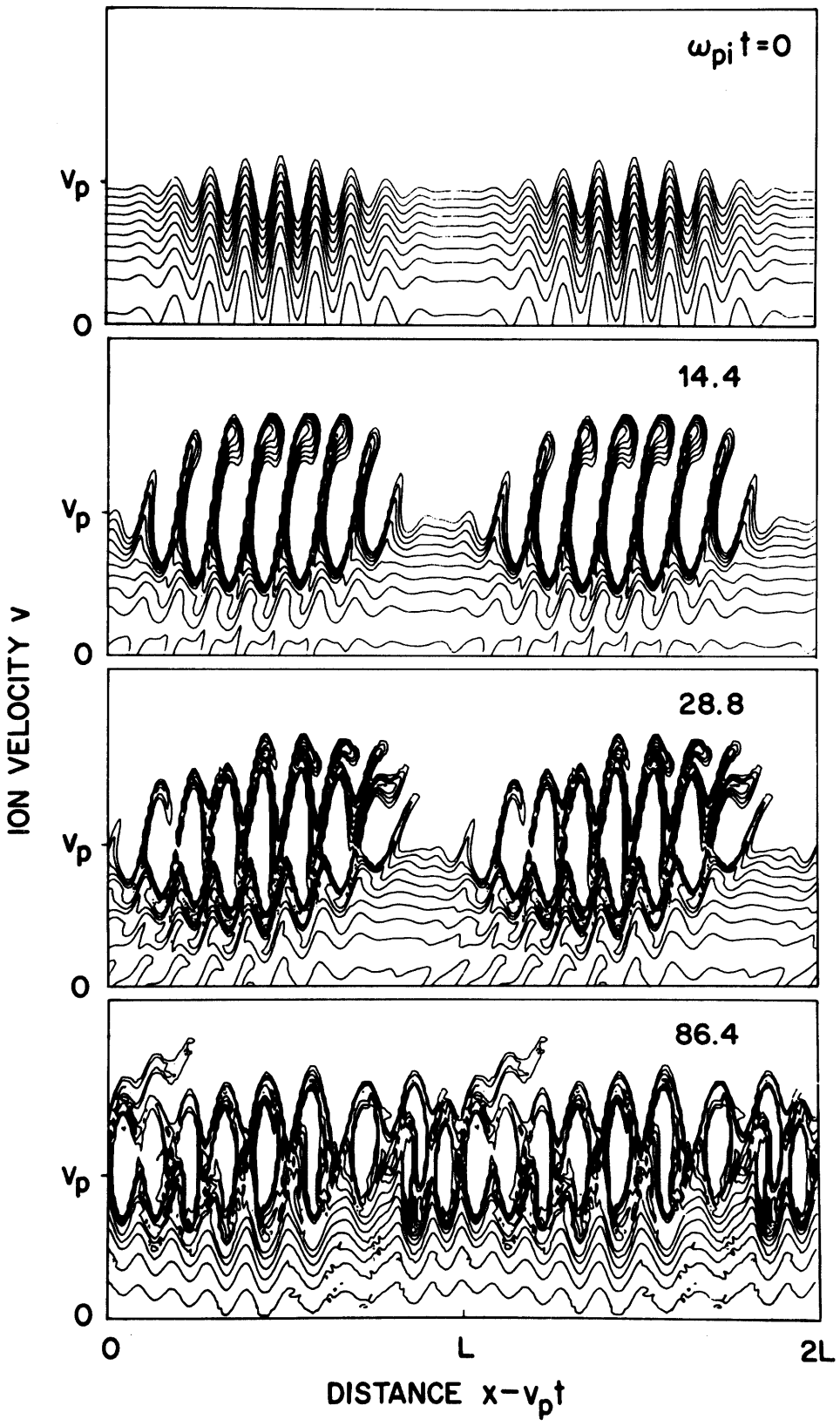

Figure 10

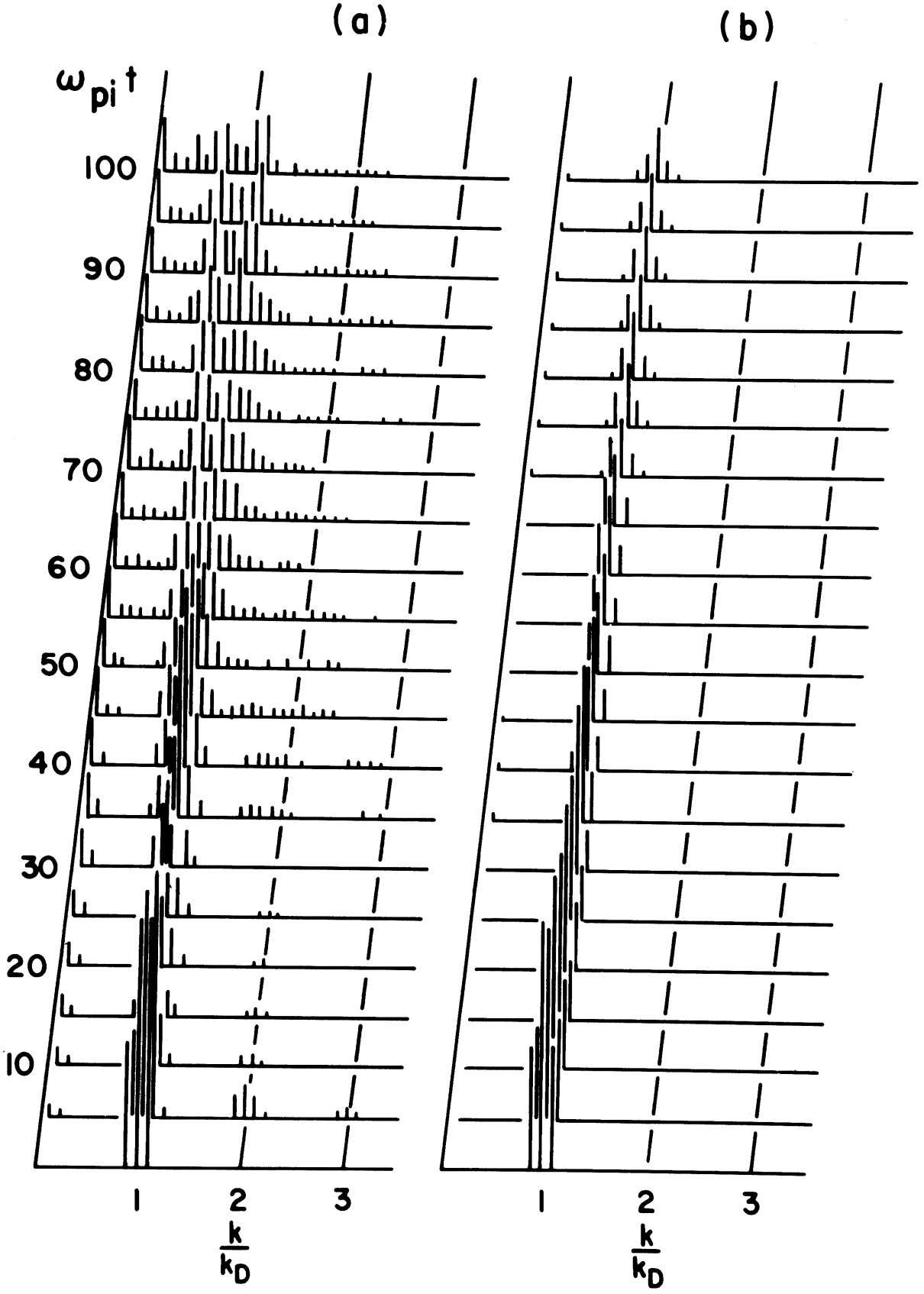

Figure 11

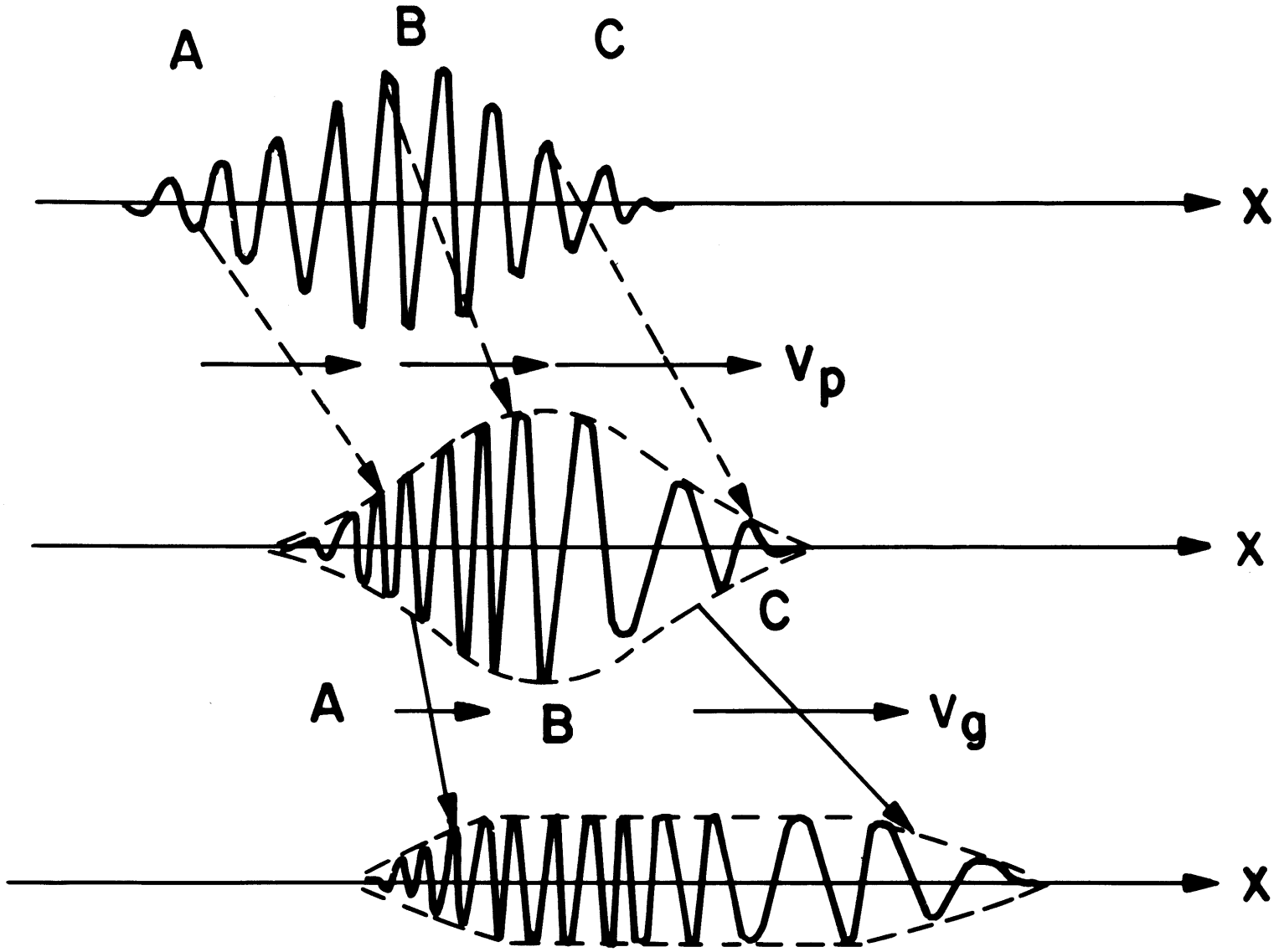

Figure 12

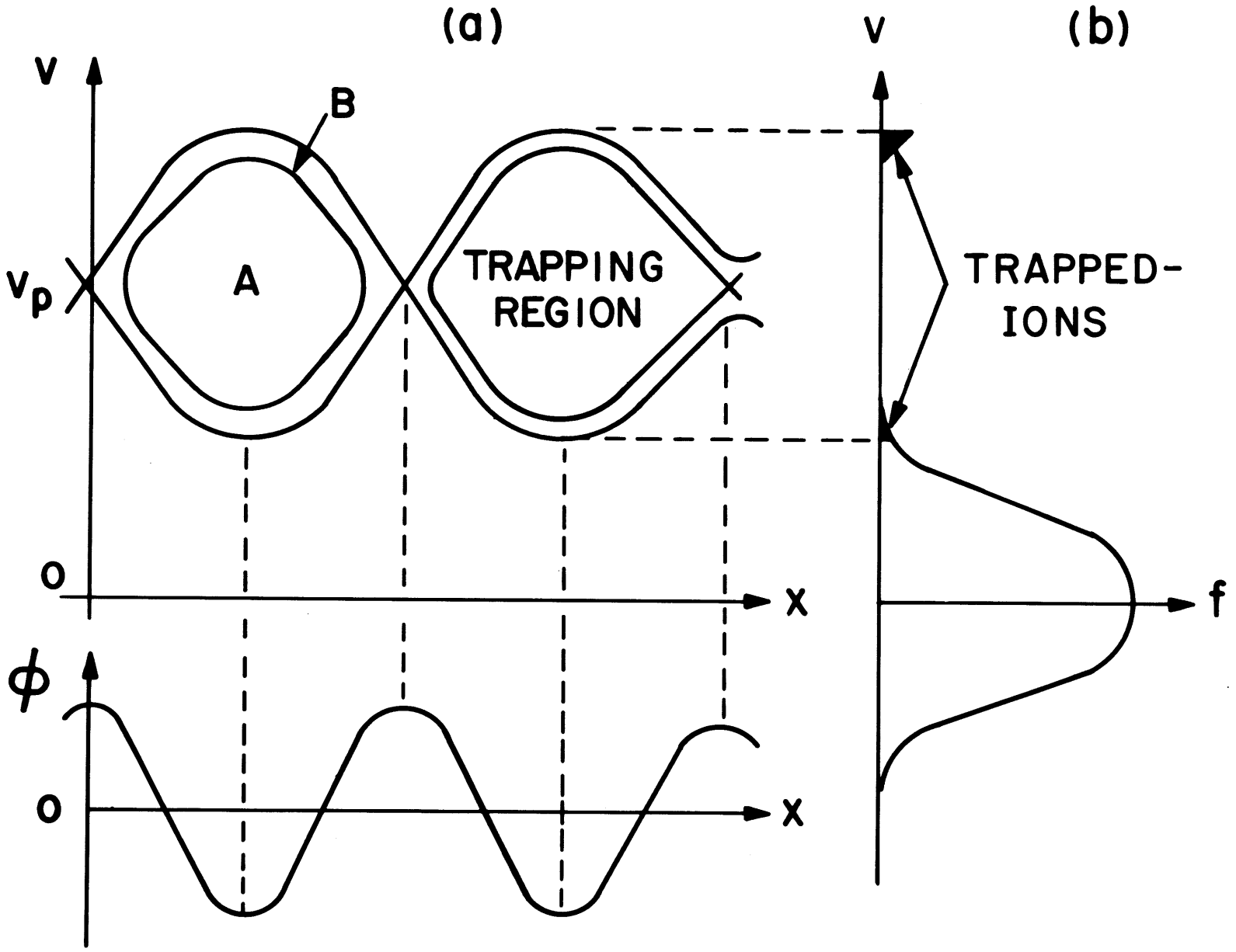

Figure 13

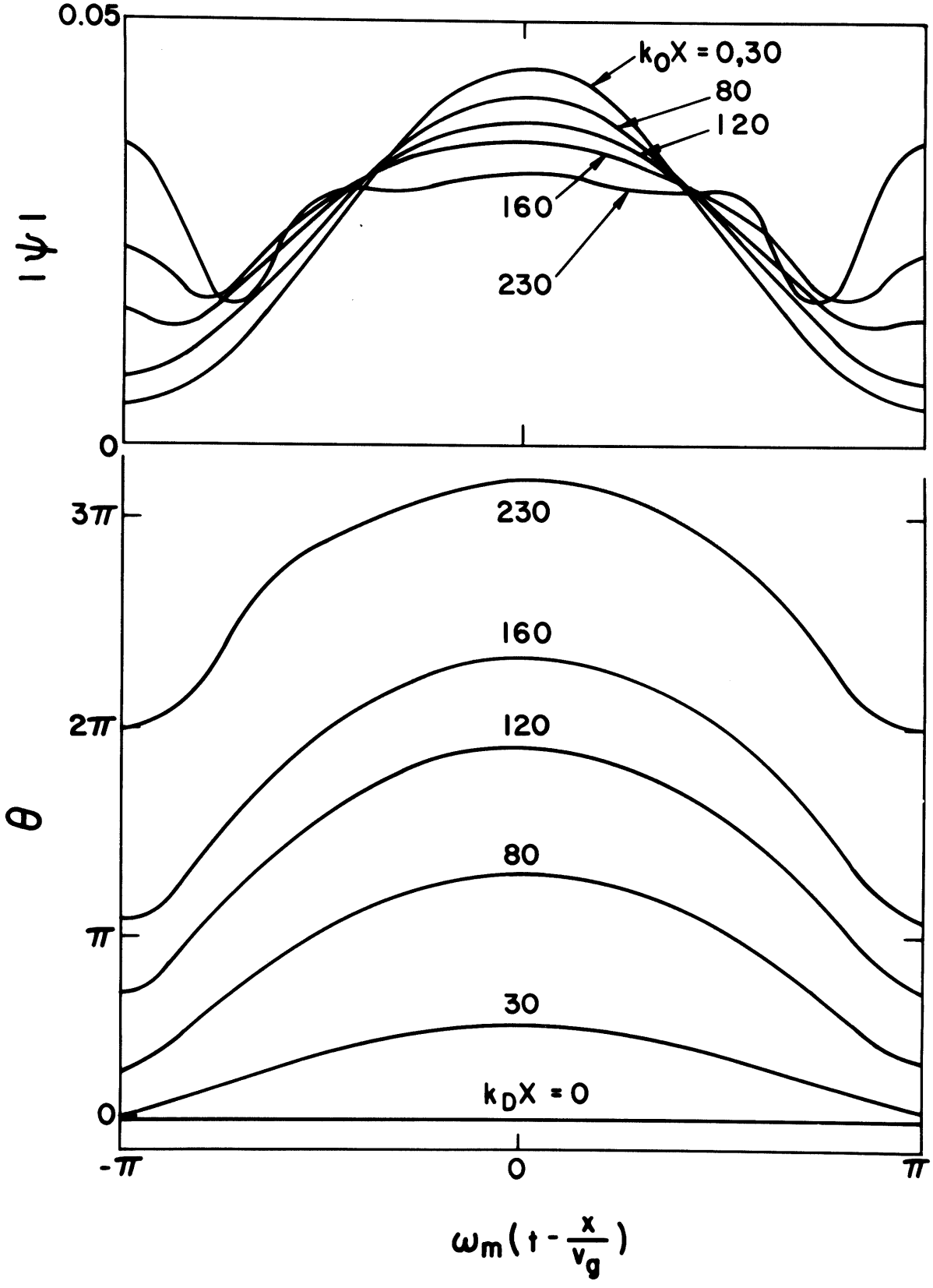
0.05
0
|ψ|
k_0X = 0,30
80
120
160
230
3π
2π
π
0
θ
230
160
120
80
30
k_DX = 0
-π
0
π
$\omega_m(t-\frac{x}{v_g})$

Figure 14

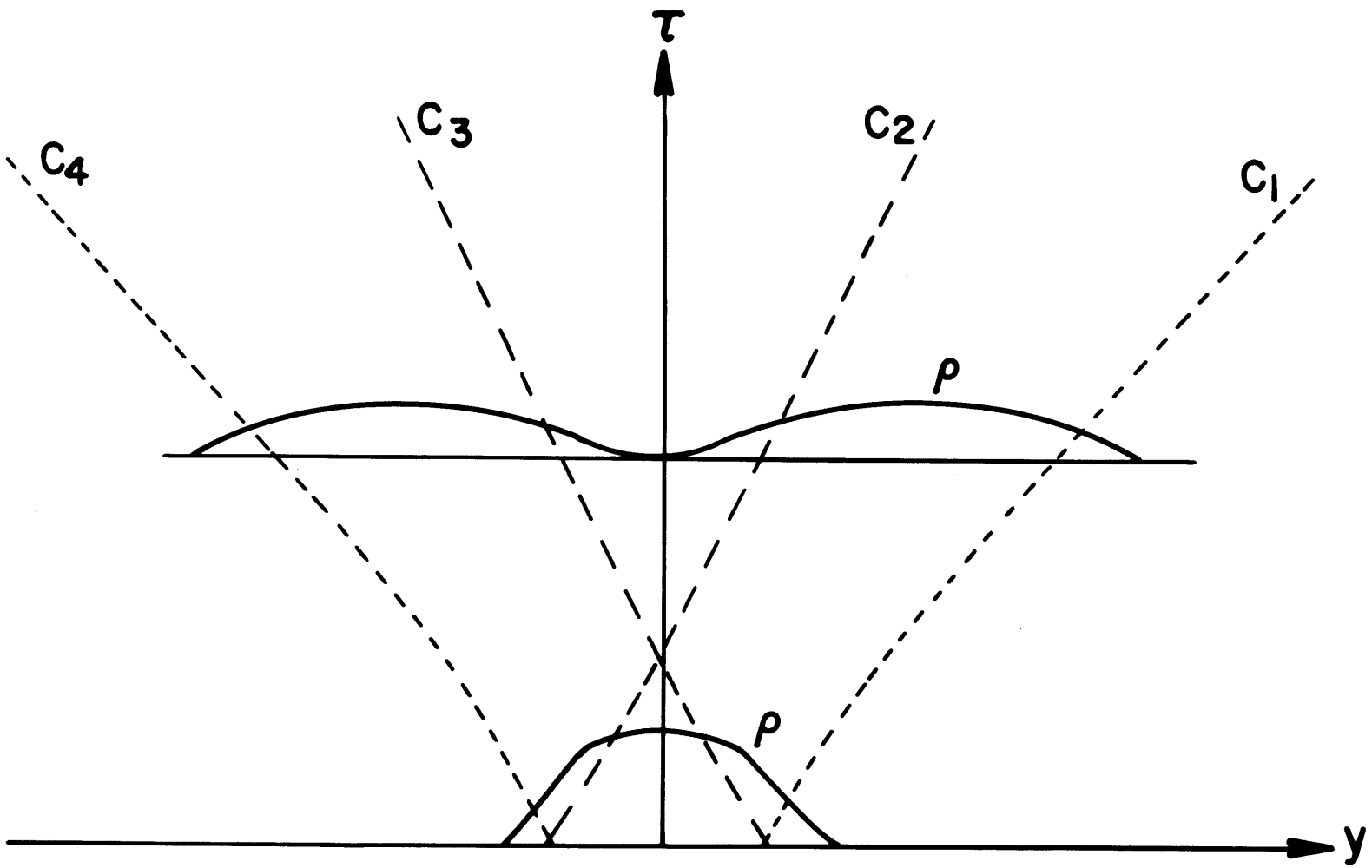

Figure 15